Case Studies in Construction Materials 19 (2023) e02258

Contents lists available at ScienceDirect

Case Studies in Construction Materials

journal homepage: www.elsevier.com/locate/cscm

Development of $Ca(OH)_2$-based geopolymer for additive manufacturing using construction wastes and nanomaterials

Youssef Mortada [a,b,*], Eyad Masad [a,c], Reginald B. Kogbara [a,d], Bilal Mansoor [a,b], Thomas Seers [e], Ahmad Hammoud [a], Ayman Karaki [a]

[a] Mechanical Engineering Program, Texas A&M University at Qatar, P. O. Box 23874, Doha, Qatar
[b] Department of Materials Science and Engineering, Texas A&M University, 575 Ross Street, College Station, TX 77843, USA
[c] Zachry Department of Civil & Environmental Engineering, Texas A&M University, College Station, TX 77843, USA
[d] Department of Environmental Engineering, Izmir Institute of Technology, Gulbahce, Urla, 35430 Izmir, Turkey
[e] Petroleum Engineering Program, Texas A&M University at Qatar, P.O. Box 23874, Doha, Qatar

ARTICLE INFO

Keywords:
Additive Manufacturing
Geopolymer
Sustainability
Waste
Nanomaterial

ABSTRACT

Recent growth in additive manufacturing (AM) or 3D printing in the construction field has motivated the development of various materials that vary in its composition and properties. This paper introduces, characterizes, and evaluates the performance of a sustainable and environmentally friendly geopolymer mixture composed of construction wastes. The geopolymer mixture has calcium hydroxide ($Ca(OH)_2$) as the main alkaline activator and incorporates nanomaterials such as nano-silica and nano-clay to enhance its suitability for AM. The combined use of $Ca(OH)_2$ for alkali activation, and nanomaterials for tailoring the behavior of construction wastes for 3D printing, is novel and addresses the shortcomings of conventional alkaline activators. The paper includes the outcomes of the analysis of the mechanical properties, printability, and microstructure of the geopolymer mixture. The 28-day compressive strength of the mixture reached 42 MPa with ambient temperature curing, which is comparable to traditional geopolymers. The inclusion of 1 wt % of nano-silica accelerated the geopolymerization process and led to the largest (35 %) reduction in the setting time. Similarly, incorporating 1 wt % of nano-clay led to reduction of the thermal conductivity from 0.709 W/mK to 0.505 W/mK, due to the introduction of thermal barriers. The printability of the studied waste-based geopolymer mixture was validated through the successful fabrication of a 3D-printed model.

1. Introduction

The construction sector is one of the most resource-intensive industries in the world, where it is responsible for 40 % of global energy utilized and 40 % of global material resources consumed [1,2]. This has presented the industry with numerous challenges in terms of managing the cost and environmental impact of construction materials and waste. It is estimated that more than 10 billion tons of construction waste is generated annually, which is approximately 25 % of total generated waste worldwide [3,4]. Concrete,

* Corresponding author at: Mechanical Engineering Program, Texas A&M University at Qatar, P.O. Box 23874, Doha, Qatar.
E-mail addresses: mortada@tamu.edu (Y. Mortada), eyad.masad@qatar.tamu.edu (E. Masad), regkogbara@cantab.net (R.B. Kogbara), bilal.mansoor@qatar.tamu.edu (B. Mansoor), thomas.seers@qatar.tamu.edu (T. Seers), ahmad.hammoud@qatar.tamu.edu (A. Hammoud), ayman.karaki@qatar.tamu.edu (A. Karaki).

https://doi.org/10.1016/j.cscm.2023.e02258
Received 26 April 2023; Received in revised form 20 June 2023; Accepted 25 June 2023
Available online 27 June 2023

bricks, soil, and asphalt make up the non-hazardous portion of construction and demolition waste (CDW), which are usually disposed of through landfill. Recycling construction materials can reduce energy consumption and reduce demand for minable natural resources [4]. Moreover, the scarcity of materials required for concrete production in some locations, such as gravel and sand, means that identifying alternative aggregates is attractive [5,6].

The environmental impact of the construction industry extends further than the quantity of resources used, or the waste generated, with studies suggesting that the production of Portland cement contributes up to 8 % of global carbon dioxide (CO_2) emissions [7]. Portland cement is the main component in traditional concrete, and due to its significant contribution to anthropogenic greenhouse gas emissions, efforts to find a replacement activator are ongoing [8]. Produced by combining aluminate and silicate materials (typically fly ash or slag) with an alkaline activator, geopolymer-based concrete has been proposed as a viable substitute for conventional concrete. Because the primary materials in geopolymers, are aluminosilicate-rich waste materials, geopolymer concrete offers a sustainable construction material [9]. Adopting geopolymers can reduce related greenhouse-gas emissions and energy consumption by up to 70 % and 40 %, respectively [10]. In addition, numerous studies have shown that geopolymers possess desirable properties when compared to standard concrete, such as corrosion and fire resistance, reduced shrinkage, lower thermal conductivity, and lower porosity [11–13]. Geopolymers can be manufactured from a wide range of materials, including waste materials like metakaolin, fly ash, and slag [14–16], reducing the need for landfill.

Many studies, in recent years, have made efforts to use recycled materials within the domain of geopolymer technology, underpinning a move towards more sustainable and resilient material construction. Among these efforts is the incorporation of recycled Polyvinyl Chloride (PVC) and glass waste into the geopolymer matrix, an approach to enhance thermal resistance and increase energy absorption [17]. The research also investigated the use of recycled PVC and rubber to enhance other key properties. It was observed that PVC can improve both the compressive and flexural strength of geopolymers and rubber showed promise in reducing the thermal conductivity and decreasing the volume of permeable voids [18–20]. Other works also considered incorporation of poly-vinyl alcohol fibres, attapulgite nanoclay, and calcined halloysite clay as low-cost additives for 3D printable alkali-activated materials [21,22]. These advances collectively reflect a commendable commitment towards both environmental sustainability and performance enhancement of geopolymer technology.

Additive manufacturing (AM) of concrete carries notable advantages over traditional concrete forming approaches, provide greater geometric flexibility in construction design, whilst potentially reducing total construction costs by 35–60 % [23,24]. Additionally, AM based concrete fabrication results in lower waste production when compared to traditional manufacturing methods. Therefore, as the implementation of AM in the construction industry grows, the environmental impact associated with concrete production and disposal can be significantly reduced. Furthermore, the need to reduce the cost and carbon footprint of projects over their operational lifespan has led to efforts to innovate towards more energy-efficient building designs [25]. Consequently, the development of thermally efficient materials represents a major challenge for the construction sector [26–28]. Hence, the present study aims to develop geopolymer materials suitable for concrete additive manufacturing, improving the sustainability of concrete construction whilst reducing waste. The study also aims to improve the thermal and mechanical properties of geopolymers using nano-material additives.

1.1. Geopolymerization

Geopolymerization comprises multiple stages: namely, destruction, coagulation, condensation and crystallization, all of which

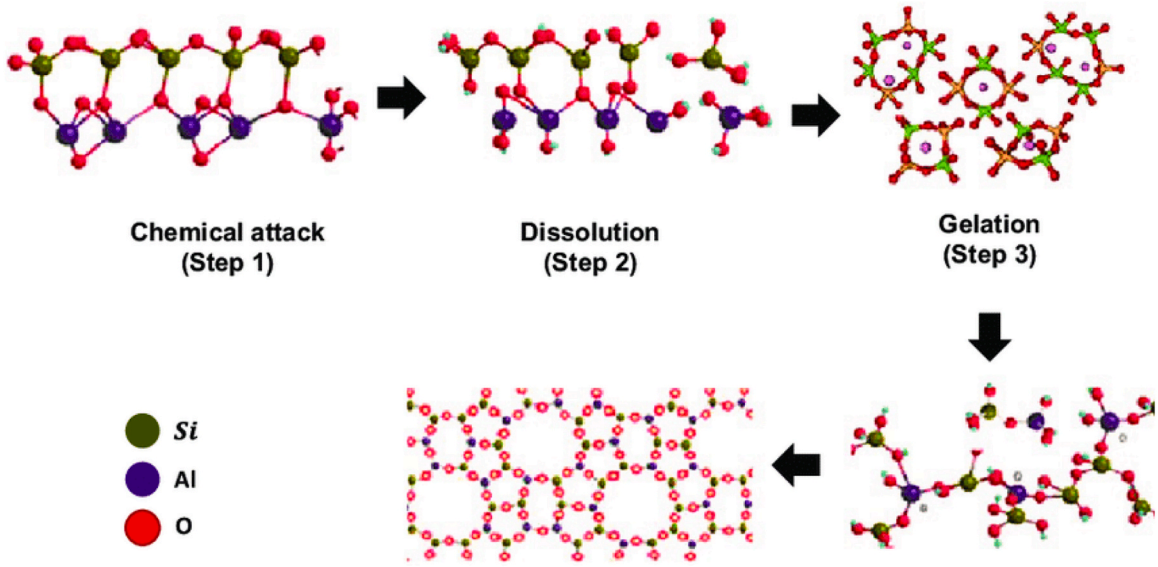

Fig. 1. Mechanism of geopolymerization reaction [31].

occur after mixing an alkaline activator with an inorganic aluminosilicate-rich material (e.g. slag / fly ash). During the destruction stage, the aluminate and silicate minerals in the inorganic material dissolve due to the high pH of the alkaline activator. The dissolution of Si-O-Si, Al-O-Al, and Al-O-Si bonds yields aluminate and silicate components, which act as free anionic monomers [29,30]. This dissolution of the bonds is attributed to the change in ionic strength of the medium, due to the electron donation from the alkaline activator. Consequently, the electronic density around the Si and Al atoms is redistributed, resulting in increased susceptibility of bond rupture [30]. Subsequently, the accumulation of monomers leads to the formation of a coagulated structure through polycondensation, which in turn precipitates into a gel. During this gelation process, a polymerization reaction begins to take place between the Al and Si monomers, forming secondary alternating tetrahedron bonds [30]. The three-dimensional tetrahedra matrix formed from polycondensation has an empirical formula of $Mn[-(SiO_2)z-AlO_2]n.wH_2O$, where n is the polycondensation degree, z & w are balancing terms, and M is the cation from the alkaline activator, which balances the charges of the anionic monomers [31]. During the polymerization reaction, Al-O groups dissolve at a faster rate than the Si-O groups due to Al-O groups having weaker bonds. This results in the Si-O dissolution step being rate-controlling for the formation of polymeric networks that are characterized by a high content of Si in comparison to Al (Si/Al $\approx$2) [30]. As the polymerization reaction and generation of additional polymeric networks continue, the crystallization of the amorphous alkali aluminosilicate gel (M-A-S-H) structure initiates. The composition of the crystallized products is determined by the mineralogical composition of the initial phase, the alkaline component's properties and curing conditions [30]. A visual representation of this geopolymeric reaction is illustrated in Fig. 1.

As the alkaline activator provides the basicity for the geopolymerization reaction to occur, the selection of the alkaline activator for geopolymerization is critical. The most prominent alkaline activators are Sodium (Na)/Potassium (K)-based, such as Sodium Hydroxide (NaOH) and Potassium Hydroxide (KOH). NaOH causes high early-age strength gains in geopolymers, although it tends to exhibit lower long-term strength gains when compared to other alkaline activators, such as KOH [31]. This increased strength is a result of KOH's greater potential for dissolution of aluminosilicates which is due to its high alkalinity when compared to NaOH [32]. Although Na/K-based activators are the most common alkaline activators, there have been rising safety concerns pertaining to their usage [32], due to their caustic nature which makes them corrosive and thus hazardous to handle. Moreover, Na/K-based activators are relatively expensive and require special preparation for use in geopolymers, potentially making them impractical for applications involving large-scale concrete fabrication.

Though calcium hydroxide ($Ca(OH)_2$) additives have been found to increase the compactness and compressive strength of geopolymers; scarce literature is available for utilizing it as the sole alkaline activator due to its low reactiveness in the polymerization process [33]. There have been recent efforts made towards the implementation of $Ca(OH)_2$ along with sodium carbonate (Na_2CO_3) [34,35]. The use of $Ca(OH)_2$ as the sole activator in geopolymers has the benefits of improving durability and eliminating the need for thermal treatments. Moreover, $Ca(OH)_2$ has a lower pH than Na/K-based activators, making it more environmentally and storage-friendly. Additionally, it is less expensive, less toxic due to its lower leachability, and easier to use, as no special preparation is required, and can be used in the form of powders directly [36,37].

Some concerns may arise regarding the environmental impact of $Ca(OH)_2$ production, which is accompanied by the release of carbon dioxide into the atmosphere during the calcination of Calcium Oxide (CaO), which is later hydrated to form $Ca(OH)_2$. However, unlike Portland cement, lime-based materials (i.e. CaO & $Ca(OH)_2$) have been found to be suitable for carbon dioxide capture from ambient air via carbonation process [38], with both calcium oxide and calcium hydroxide possessing high levels of carbonation reaching approximately 75 % from ambient air within practical time scales of weeks to months [38]. In [38], a process utilizing carbonation was presented which is economical and does not require the need for costly equipment or reactors. Moreover, [39] presented a combined process for heat, power, and CaO generation that achieves negative emissions. This process exploits revenues from the power, heat, and lime industries making it both competitive with standalone technologies and economically feasible [39]. Consequently, though the formation of $Ca(OH)_2$ releases CO_2, it also offers the possibility to remediate carbon dioxide emissions through carbonation, thus making it potentially less environmentally impactful than Portland cement.

1.2. Nano-materials additives

Integration of nanotechnology into the construction field has attracted considerable interest with specific nano-materials modulating the properties of cement-based and cement-free materials. Nano-materials are used to address issues related to durability [40], physical structure [41], and thermal-mechanical properties [42]. Nano-materials, such as nano-silica [43,44], nano-clay [45–48], and titanium dioxide [49], could be introduced to cement-free materials, such as geopolymers, to improve their properties. For example, nano-clay was used as a replacement for lightweight aggregates (e.g., expanded perlite) to improve the thermal properties of geopolymers without sacrificing strength [50]. Typically, the incorporated percentage of nano-clay in geopolymers ranges between 1 and 5 wt % [50–54], where the addition of >2 % wt % nano-clay offers measurable improvement in the flexural/compressive strength and hardness of geopolymers. Nano-clay has also been added in small dosages (1–1.5 wt %) to enhance the thermal properties of geopolymers, where the thermal conductivity of the geopolymer decreases with the addition of up to 1.5 wt % of nano-clay, with a noticeable increase occurring at fractions [53]. Conversely, nano-silica is used to increase the polymerization reaction rate, owing to its large surface area, which allows it to fill the smaller voids present in the geopolymer structure [55–57]. The addition of 1–5 wt % nano-silica has been found to decrease the initial and final setting time of geopolymers, as well as to increase the viscosity of geopolymer mixtures in their fresh state [36,55]. The decrease of the setting time of a material provides an advantage for AM technology since this would promote a faster rate of strength gain and better shape stability for the initially deposited layers. It also makes the printing material amenable to more recent commercially available 3D printers with simultaneous mixing and extrusion of materials that requires fast-setting cementitious materials. In addition to enhancing material properties, nano-materials have also been used to

modify geopolymer mixtures to improve printability characteristics, such as shape retention and buildability [58].

This study presents a novel geopolymer mixture, which uses $Ca(OH)_2$ as the sole alkaline activator, with construction and demolition waste utilized as a sustainably sourced aggregate. It also assesses the impact of nano-silica and nano-clay additives for improving geopolymer setting time and thermal properties. The combined use of $Ca(OH)_2$ for alkali activation, and nanomaterials for tailoring the behavior of construction wastes for 3D printing, is novel and addresses the shortcomings of conventional alkaline activators. Further, the ability to modify the setting time of the geopolymer would make it a more suitable candidate for AM applications irrespective of the changing material requirements of each print. Moreover, the improvement of the thermal properties, through the reduction of the thermal conductivity, would enhance the overall energy efficacy of a geopolymer structure during its life cycle. Finally, the printability of this eco-sustainable geopolymer is assessed for its feasibility to be used in AM.

2. Materials and methods

2.1. Materials

$Ca(OH)_2$ was utilized as the alkaline activator for the geopolymer mixture investigated herein. Ground granulated blast-furnace slag (GGBFS) is a silica-rich by-product from the metallurgical industry, which is utilized as the aluminosilicate-rich precursor. Gypsum was used as a dehydrating agent to absorb excess water and improve the strength of the geopolymer mixture. Moreover, clay brick and concrete waste generated from construction and demolition were integrated into the geopolymer material design. Aggregates from both waste material sources were introduced to improve the strength, durability, and thermal properties of the geopolymer. The clay brick was also used in powder form as an additional aluminosilicate source for the formation of the geopolymer binder. Superplasticizer Hyperplast-ES910i (H-ES910i) was added to the water to reduce the water–cement ratio, improving the mechanical properties and flowability of the geopolymer mixture.

Several mixtures with different waste content percentages were investigated to determine the maximum waste that can be incorporated whilst maintaining acceptable mechanical properties under ambient curing conditions. Table 1 lists the constituents and the corresponding proportions for each of the investigated mixtures. The optimum geopolymer mixes were found to be the ones with 1 % nano-clay (NC) (identified as the lowest thermal conductivity in Sections 3.1.2) and 1 % nano-silica (NS) (identified as the fastest setting time in Section 3.2.1).

The GGBFS was grounded into a fine powder, then sieved through a 75-μm diameter aperture sieve. Concrete and brick wastes were obtained from three randomly selected demolishing sites within Qatar. The wastes were then crushed and separated into two aggregate sizes via sieving. These were denoted as aggregate group A with particle sizes $<500\ \mu$m, and aggregate group B with particle sizes in the range, 500–2000μ m. The particle size distribution for aggregate group A and B can be seen in Fig. 2. $Ca(OH)_2$ and H-ES910i were sourced by Don Construction Products Qatar. Kaolin NC and NS were obtained from Nanoshel, LLC (India). The particle size for NC and NS ranged from 40 to 80 nm and 15–20 nm respectively. Gypsum was sourced locally from Qgyps Gypsum Board Factory (Qatar).

2.2. Sample preparation

Aggregates A were initially mixed together before being ground for two minutes. The grinding step was introduced in order to increase the surface area of the cementitious powders to enhance the compressive strength of the resultant geopolymer [32,59]. To assess the impact of aggregate comminution on geopolymer properties, base mixtures (0 % nanomaterial) were prepared with and without grinding. A particle size analyzer (using ASTM C204) was used to measure the specific surface area of these base mixtures, which increased from 3827 to 5103 cm^2/g after grinding. Moreover, the grinding process was found to improve the strength of the slag-based geopolymers by around 5 MPa at 7 days post-curing. In mixtures incorporating nano-material (NM) additives, NMs were added after the grinding of the group A aggregates, and an additional one minute of grinding was performed. Subsequently, all aggregates were placed in the Hobart N50 5-quart (4.7 L) mixer at the low-speed setting, with water and superplasticizer added. The mixing speed was then increased to the medium setting for one minute. After this period, the mixer was stopped, and the sides of the

Table 1
Geopolymer mixture proportions.

Material	Mixture Composition (kg/m^3)	Geopolymer Mixtures						
		0 % NM	1 % NC	2 % NC	3 % NC	1 % NS	2 % NS	3 % NS
Aggregates A (<500 μm)	Gypsum	60	60	60	60	60	60	60
	Calcium hydroxide	378	378	378	378	378	378	378
	GGBFS	490	490	490	490	490	490	490
	Solid brick powder	60	60	60	60	60	60	60
Aggregates B (500–2000 μm)	Concrete aggregate	872	872	872	872	872	872	872
	Solid brick aggregate	132	132	132	132	132	132	132
Liquids	Water	290	290	290	290	290	290	290
	H-ES910i	8	8	8	8	8	8	8
Nanomaterials	Nano-silica (NS)	0	0	0	0	5.3	10.6	15.9
	Nano-clay (NC)	0	5.3	10.6	15.9	5.3	5.3	5.3

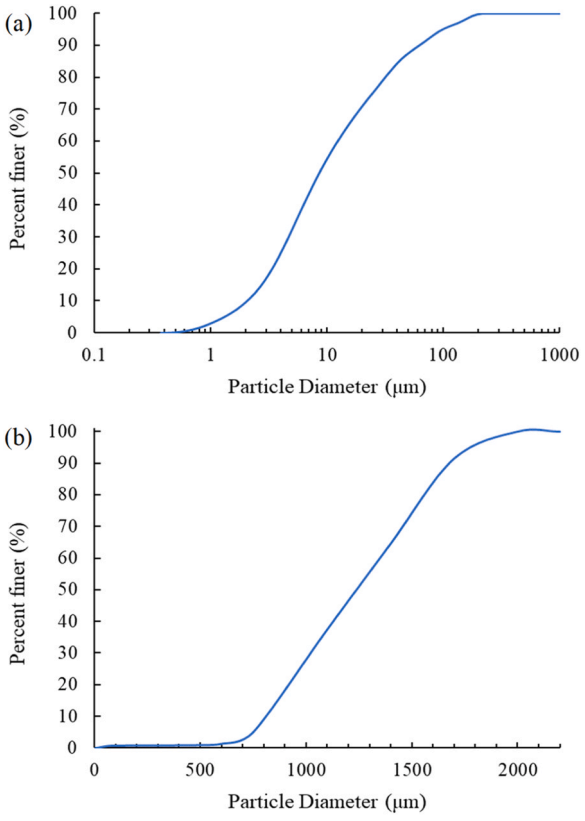

Fig. 2. particle size distribution for (a) aggregate group A and (b) aggregate group B.

mixer bowl were scrapped manually for 30 s to ensure that all the material adhering to its sides were fully incorporated, followed by an additional one minute of mixing us at the medium-speed setting. Finally, the material was extracted from the mixer to either be placed in molds for testing or used in 3D printing. Fig. 3 summarizes the sample preparation process.

2.3. Geopolymers properties

2.3.1. Compressive strength

Compressive strength tests were conducted using the MTS 810 material test system, equipped with the MTS 609 alignment fixture

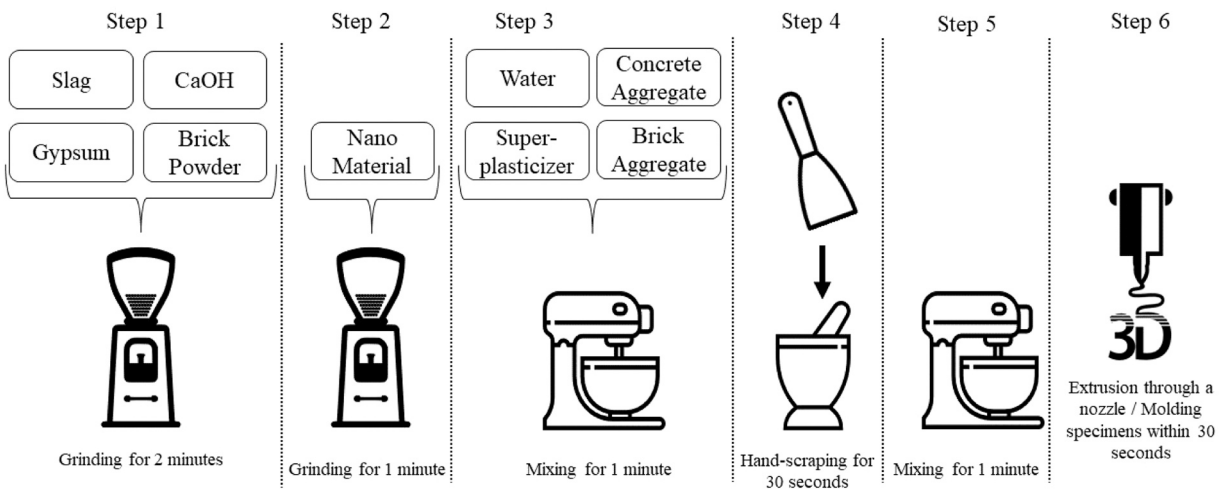

Fig. 3. Flowchart of material preparation.

and MTS 643 compression platen. Compressive tests were conducted on geopolymer samples cured for 7 days and 28 days using the ASTM C109/C109M standard with a loading rate of 0.9 kN/s [60]. Compressive strength tests were conducted three times for each material.

2.3.2. Thermal conductivity

Thermal analysis for the geopolymer mixtures was conducted using the Thermtest transient line source and its standard 50-mm sensor. The test was conducted on 50 mm diameter, 70 mm long cylindrical samples. After a 50-mm-deep hole was drilled in each of the samples using a 4-mm drill bit, thermal grease was applied to enhance the contact between the sample and the sensing probe. Over the test's duration (three minutes), a thermal gradient was induced in the specimen by passing heat in a uniaxial path through the test specimen [61]. Three thermal conductivity samples were tested for each of the mixtures according to the ASTM D5334 standard test method [62].

2.3.3. Microstructure analysis

2.3.3.1. Scanning electron microscope (SEM) analysis. Scanning electron microscope (SEM) analysis was carried out to capture the microstructural images of the specimens 28 days after preparation. Thermo-Fisher Lumis SEM operated in electron backscatter diffraction (EBSD) mode was used along with a T2 detector using a metal-oxide semiconductor sensor. The probe was set to the 'Immersion' use case at 3.00 kV, 6.3 pA, and X80k magnification. The concrete samples were coated with a 15-nm lining of platinum to prevent charging of the samples, which can lead to thermal damage and charging artifacts within the resultant images.

2.3.3.2. X-ray micro-computed tomography (X-ray μCT) analysis. X-ray μCT images of the geopolymer samples were captured using a Thermo-Fisher HeliScan μCT scanner to evaluate the macro-porosity of each sample. The test was carried out on three different cylindrical samples per mixture (48 mm × 24 mmø). Images were captured using a space-filling protocol and large spot size, with x-ray tube voltage set to 120-kV and a current of 55-mA. A 100-μm steel filter in front of the x-ray source was used to reduce beam hardening.

2.3.3.3. ASTM porosity analysis. The porosity of the geopolymer samples was also measured following the ASTM C642–21 method. Each sample was heated in an oven at 110 °C for 24 h and then soaked in water for 48 h. The difference between the oven-dry mass and the saturated mass after immersion represents the porosity of the sample (maximum water absorption) [63]. The test was carried out on three different cylindrical samples per mixture (48 mm × 24 mmø).

2.4. Printability analysis

Printability in additive manufacturing refers to the material properties required successful printing. Mortada et al. [64] proposed a set of standardized and nonconventional tests in an attempt to assess the printability of concrete mixtures in terms of three attributes: setting time, flowability, and buildability.

Setting time is defined as the duration that elapses from the initial contact between water and cementitious materials to the point at which the concrete has formed sufficient hydration products to become a solid material. *Flowability* is defined as the ease with which the material can be poured or pumped without any breakage or disruptions in the deposited layers. *Flowability* is defined in terms of the shear yield strength profile measured in a rheology test over time. In this regard, two bounds are defined, with the lower bound of the shear stress being a function of the desired layer thickness, and the upper bound being defined as the shear stress at the time when flaws (e.g., cracks and gaps) start to appear in the deposited layers. The final printability attribute of a printable mixture is its *buildability*, which is the ability of the layers of material that are deposited during the printing process to gain sufficient strength to support the weight of subsequent layers without collapsing. As buildability is a material-specific property that varies with the selected print settings, in this work it was determined by measuring the early-age compressive strength of the mixture. In this section, test methods

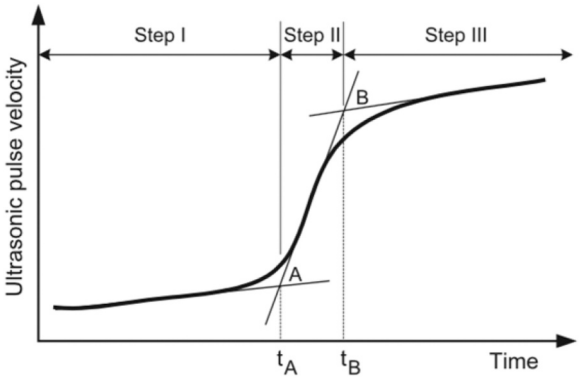

Fig. 4. Evolution of the UPV of cementitious material as a function of time [65].

discussed by Mortada et al. [64] are used to characterize the fundamental printability of the proposed geopolymer mixtures; while taking into consideration that other factors (print time, size, geometry, etc.) should be accounted for when large-scale prints are targeted.

2.4.1. Setting time analysis

2.4.1.1. Ultrasonic pulse velocity test. An earlier study utilized ultrasonic pulse velocity (UPV) tests for measuring and assessing the setting time of concrete mixtures [64]. The UPV test is a nondestructive method used to continuously monitor the hydration reaction of concrete and assess setting times [64]. The UPV test uses a transducer and receiver module placed in direct contact with a fresh geopolymer concrete sample. The transducer emits a longitudinal pulse wave, which is transmitted through the concrete sample until it reaches the receiver on the opposing end of the sample. The evolution of wave velocity is recorded and plotted. Fig. 4 shows an idealized UPV evolution with time, where the inflection point A represents the setting time of the concrete sample [64].

The Pundit Pl-200 with a 54-kHz transducer/receiver system by Proceq SA of Schwerzenbach, Switzerland, was used to measure and monitor the evolution of the UPV for the studied geopolymer samples. Fresh concrete was poured into the mold, where it came in direct contact with the transducer and receiver modules. Upon initiation of the test, UPV values were recorded every five seconds. Fig. 5 shows the corresponding experimental setup.

2.4.1.2. Vicat needle test. The Vicat needle test is an ASTM standard test for the setting time of concrete. This is a discrete and destructive test, where the setting time is determined following the ASTM C-191 standard [66]. In this work, the standard testing procedure was modified to find the penetration depth of the needle after every 30-second interval after leaving the geopolymer sample in the mold undisturbed for three minutes. Fig. 5 shows the Humbodlt Manufacturing Vicat needle used to conduct this test.

2.4.1.3. Thermal energy analysis. Concrete hydration is an exothermic reaction that can be monitored through thermal sensors to assess concrete setting time. Thermal energy release during the exothermic reaction was assessed using a thermal camera, which carries the advantage of being nondestructive and non-contact. The thermal camera detects the change in temperature throughout the geopolymerization process. Exothermic peaks in geopolymers are present at the initial stages of geopolymer setting [65], meaning that thermal energy analysis can be used for assessing the setting dynamics of geopolymers. In this study, an FLIR SC640 IR camera was used to monitor the thermal energy generated by hydration the sample, with thermal images captured at eight seconds. Thermal imaging was conducted in conjunction with the UPV test, enabling comparative analysis.

2.4.2. Flowability test

Rheological assessment of the geopolymer material was done using the Anton Paar MCR302 rheometer, equipped with a CC27/T200/SS/P measuring cell and ST22–4V-40/113 stirrer. The evolution of the shear strength of the material was assessed, assuming that the material follows the Bingham material model. Rheology tests were conducted at a constant speed of 1200 rpm, in order to imitate the mixing speed of the Putzmeister P-12 cavity concrete pump that was used to print the material. Tests of three samples were conducted for each mix in order to determine the arithmetic mean and standard deviation of shear yield strength.

The mixes were 3D printed to determine their shear strength-printability limits. The laboratory-scale concrete 3D printer setup was used in conjunction with a six-axis ABB IRB-140 robotic arm and Putzmeister P-12 cavity pump (Fig. 6). The 3D printing test entailed continuously printing single-layer filaments and assessing the thickness of these filaments. Moreover, the theoretical layer thickness was calculated, and tolerances were accounted for in order to determine the lower and upper limits of the acceptable printed layer.

3D printing parameters were the same as those used in Mortada et al. [64], with a volumetric flow rate of 112.5 cm^3/s, print speed

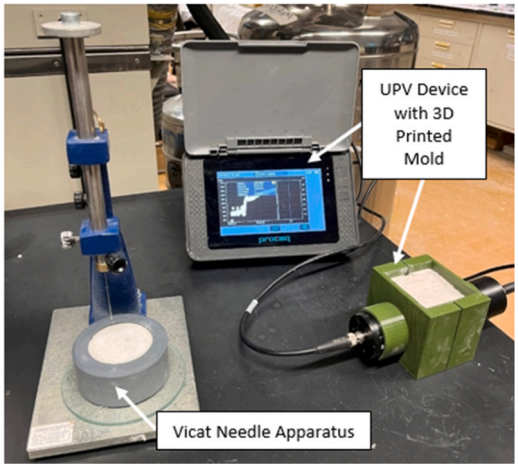

Fig. 5. Experimental setup used to measure the setting time [65].

of 18.5 cm/s, nozzle height of 2 cm, and theoretical layer thickness of 3 cm. A user-defined layer thickness tolerance of 0.5 cm was selected; with the print test's lower limit being defined as a maximum layer thickness of 3.5 cm. The upper limit of the acceptable printed layer was defined as the point at which discontinuities and/or cracks become visible within the printed layer [64].

2.4.3. Buildability test

The buildability assessment of geopolymer material conducted herein focuses on failure through plastic collapse. Thus, early-stage compressive strength is the key property that was evaluated in this regard. The MTS 810 material test system equipped with an MTS 609 alignment fixture and MTS 643 compression platen was used to determine the early-age compressive strength of the studied samples by using the ASTM C109/C109M standard with a loading rate of 0.9 kN/s [60]. The time of testing was changed such that the compressive strength tests were conducted at 9, 10.5, 15, 20, 30, 40, 45, 50, and 60 min after mixing, in order to monitor the early-age compressive strength gain in an accurate manner. Three separate trials were conducted for each testing time, with the arithmetic mean and standard deviation calculated for each test.

3. Results and discussion

3.1. Geopolymers properties

3.1.1. Compressive strength

Compressive strength was assessed at 7 and 28 days and was found to be 26 MPa and 42 MPa, respectively. Compressive strength values are comparable to other sodium-based geopolymer mixes in the literature, where the 28-day strength ranges from 40 to 80 MPa [67–69]. Additionally, the 7-day strength is comparable to waste aggregate-based geopolymers found in literature where the strength ranges from 5 to 36 MPa [17,18,70].

3.1.2. Thermal conductivity

The thermal conductivity of the geopolymer mixture (0 wt % NM) was optimized by incorporating NC from 1 wt % to 3 wt %. Three samples were tested for each of the four mixes according to the ASTM D5334 test, and Table 2 lists the average thermal conductivity values of each mix. The addition of 1 wt % NC resulted in the greatest reduction in thermal conductivity (29 %) relative to the control mix, while 2 wt % and 3 wt % reduced the thermal conductivity by 10 % and 8 %, respectively. The lowest recorded thermal conductivity was 0.505 W/mK at 1 wt % NC, a value that aligns with Na- activated geopolymers. Typically, Na-activated geopolymers display a thermal conductivity within the range of 0.65–0.95 W/mK, which can dip to 0.4–0.6 when lightweight aggregates, fibers or NC are introduced properly [71,72].

3.1.3. Microstructure analysis

3.1.3.1. Scanning electron microscope (SEM) analysis. The limited reduction of geopolymer thermal conductivity between mixtures incorporating 2 wt % and 3 wt % nano-clay was investigated further using SEM. EBSD SEM analysis of the different samples was conducted after 28 days of mixing (Fig. 7). NC particles were detected in all of the studied samples, with the quantity of clay particles present increasing from 1 wt % to 3 wt %. Flocculation of the NC particles can be observed, with some clay clusters exceeded 1 μm in size. SEM microstructural analysis showed that clay particles act as nucleation sites, with hydration products visibly extending from the matrix onto the particles themselves. The ability of the clay particles to promote nucleation and further growth of the hydration products is believed to result in a denser and more interconnected microstructure of the geopolymer mix (Fig. 7), causing reduction in porosity. Similar behavior was observed in Na/K activated geopolymers at NC dosages between 3 and 5 wt % [45–49].

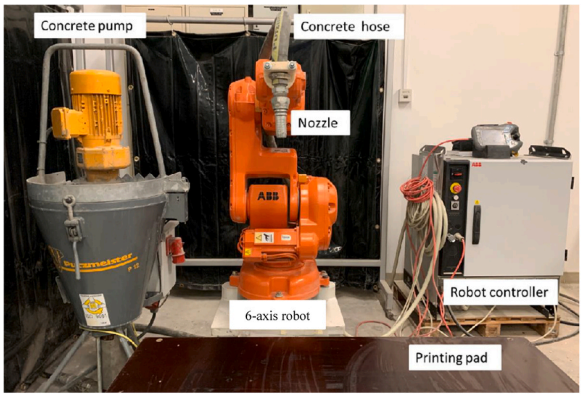

Fig. 6. Laboratory-scale concrete 3D printing setup.

Table 2
Thermal conductivity values for the mixtures with nano-clay additives.

Mixes	Thermal Conductivity (W/mK)	Percent Reduction from Base Mix
0 % NM	0.709 ± 0.002	—
1 % NC	0.505 ± 0.003	28.8 %
2 % NC	0.635 ± 0.008	10.4 %
3 % NC	0.661 ± 0.009	7.8 %

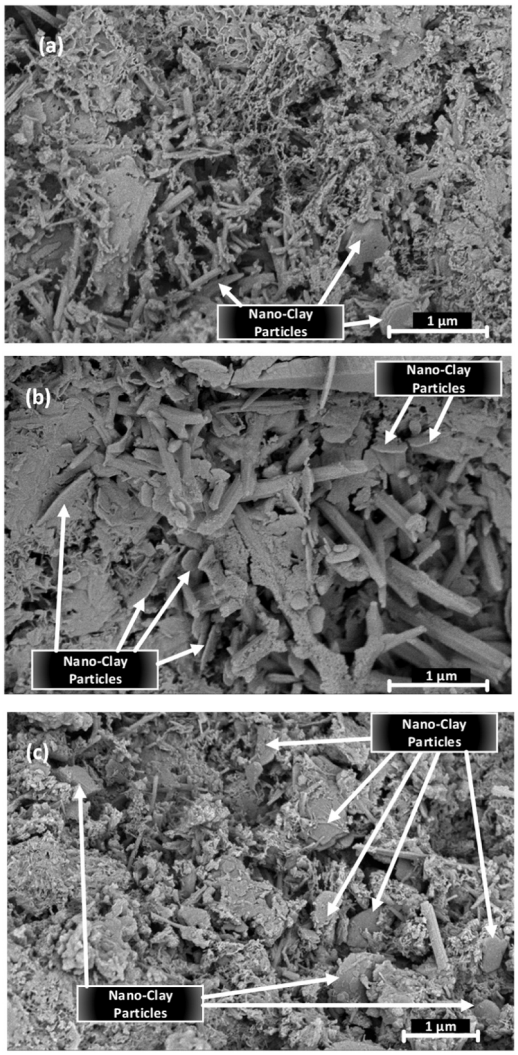

Fig. 7. SEM analysis for geopolymer with (a) 1 % NC, (b) 2 % NC, and (c) 3 % NC.

3.1.3.2. X-ray micro-computed tomography (X-ray μCT) analysis. X-ray micro-computed tomography (μCT) images of the studied the samples were captured and analyzed using the Thermo-Fisher Scientific Avizo™ software. For each sample, images were filtered using non-local means denoising [73] and an unsharp mask prior to segmentation of the pore system using adaptive thresholding. The segmented pores were then cleaned using morphological operations (morphological opening, hole filling, small spot removal). Fig. 8 presents an orthoslice for one of the μCT images for the sample with NC before and after segmentation and cleaning.

The filtered pores had a minimum and maximum equivalent diameter of 93.6 μm, and 4.09 mm, respectively. The minimum diameter (i.e. pore size) represents the detection limit for the scanned pores, which equates to the feature resolution of the scanned samples. The distribution of the pore diameters for one of the samples (3 % NC) is presented in Fig. 9, highlighting the minimum equivalent diameter. The pores were accordingly split based on the achieved feature resolution into macro pores (i.e. pores with an equivalent diameter larger than or equal to 93.6 μm) and sub-macro (SM) pores (i.e. pores with an equivalent diameter smaller than 93.6 μm).

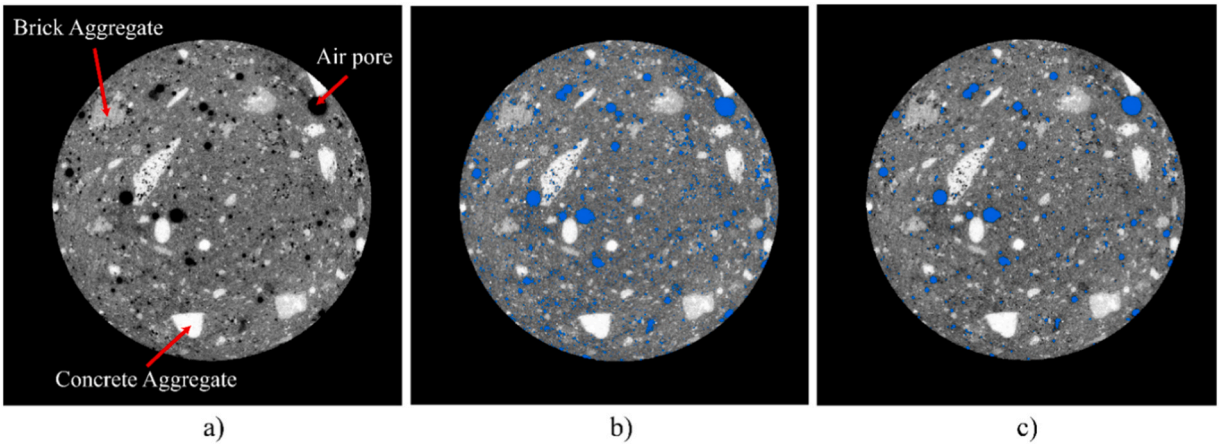

Fig. 8. Two-dimensional orthoslice rendering for the nano-clay specimen: (a) scanned image, (b) segmented air pores before filtering, and (c) macro-pores after filtering.

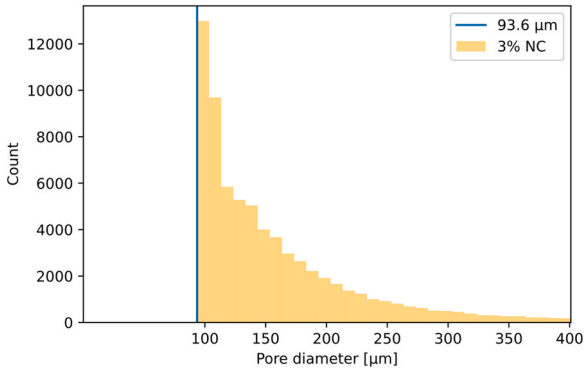

Fig. 9. The pore diameter distribution for the 3 % NC sample (ranging from 93.6 μm to 400 μm).

3.1.3.3. ASTM porosity analysis. The porosity that is contributed by the SM pores (with a diameter less than 93.6 μm) was calculated by finding the difference between the total and macro porosity. Table 3 provides the total porosity and microporosity of the studied samples.

Fig. 10 plots the porosity contributed by the macro-pores and sub-macro pores, showing a decrease in the fraction of porosity contributed by SM pores with increasing nano-clay content, with the relative contribution of the macro-porosity being constant for all samples. The decrease in the sub-macro-pore void fraction relates to NC additives predominantly acting on the walls of smaller pores, leading to the growth of hydrate products within these voids, thus promoting a more interconnected microstructure. The total porosity observed across all specimens varied from 9.60 % to 11.77 %, a figure that falls beneath the 13–17 % porosity typically seen in Na-activated geopolymers [74].

The observed increase of the thermal conductivity after the addition of >1 wt % nano-clay could relate to the enhanced micro-structural interconnectivity induced by the nucleation of hydrate products within smaller pores. As illustrated by Fig. 11, the nano-clay particles act as 'islands' that occlude sub-macro pores and act as insulation barriers due to the lower thermal conductivity of the clay particles, resulting in improved thermal properties. Conversely, introducing excess amounts of NC particles fills up more SM pores, leading to a more interconnected microstructure and a commensurate decrease in the porosity of the samples. Consequently, as the sample becomes more interconnected there are fewer pores present to disturb thermal energy flow, promoting thermal conductivity. The optimum NC dosage (1 wt %) was incorporated to the remaining mixes throughout this study.

3.2. Printability measurements

3.2.1. Setting time measurements

3.2.1.1. UPV and vicat needle test. The UPV and Vicat needle tests were employed to measure the average setting time for the base mix (0 % NM – with the addition of the optimum 1 % NC) and the three mixes with nano-silica (1 % NS, 2 % NS, and 3 % NS. For each mix, the average setting time was determined as the mean duration of three mix trials. For each trial, the evolution of the UPV with time was

Table 3
Total porosity and macro-porosity percentage for mixtures with nano-clay additives.

Mixes	Macro-pore Porosity (%)	Total Porosity (%)
0 % NM	3.15	11.77
1 % NC	3.27	10.75
2 % NC	3.34	10.10
3 % NC	3.56	9.60

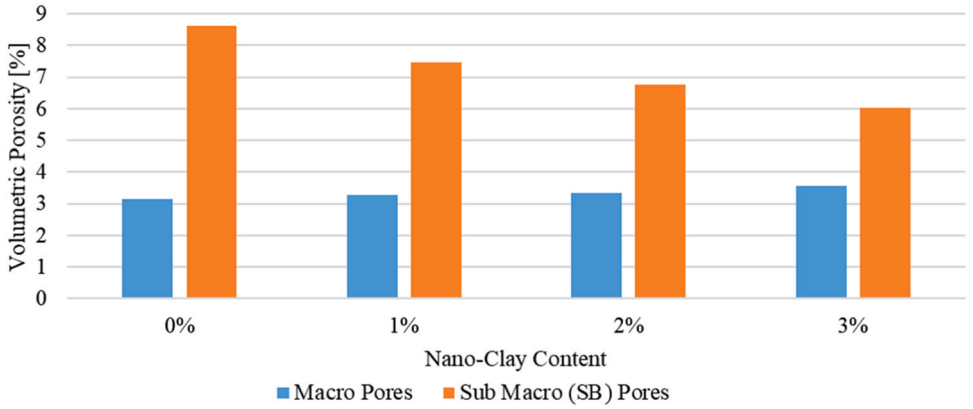

Fig. 10. Volumetric porosity percentage for the macro- and sub macro-pores for the mixtures with nano-clay additives.

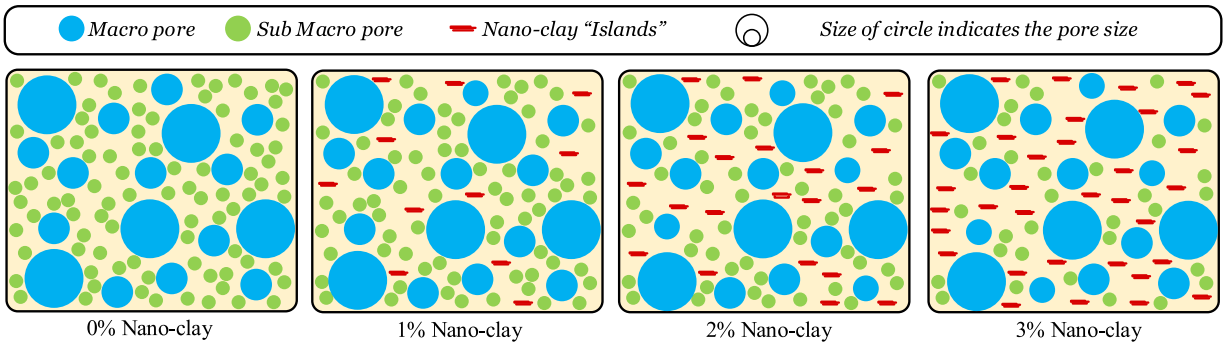

Fig. 11. Visual representation of the effect of adding nano-clay to geopolymer samples.

monitored and plotted, where the setting time was determined by the inflection point on the graph (Fig. 12). All UPV tests were initiated 3 min after the initial contact with water to allow for sufficient mixing and specimen molding.

Table 4 presents the average setting time, measured using UPV and Vicat needle tests, for each mix. Notably, the addition of nano-silica reduced the setting time of the geopolymer mix. The addition of 1 wt % of NS induced the biggest reduction (35 %), whilst 2 wt % and 3 wt % reduced setting times by 22.5 % and 12.5 % respectively. The decrement of 35 % is similar to the reduction seen in the setting time of Na/K-activated geopolymers, which could potentially be as significant as 30–42 %. [43]. The reduction of the setting time is due to the increased surface area of the solid phase and the ability of the nano-sized silica particles to fill voids within the geopolymer matrix, accelerating the polymerization reaction(e.g. Aggarwal et al. [55]; Roviello et al. [57]). The increase in the setting time from 1 wt % of NS to 2 wt % and 3 wt % is attributed to the oversaturation of the mixture with silica particles. This oversaturation delays the polymerization process, with NS acting as an unreacted precursor, reducing the efficacy of the NS additives in reducing setting time.

3.2.1.2. Thermal energy analysis. The effect of the thermal energy released during the geopolymerization process was assessed to affirm the reduction of the setting time. The change in the temperature of each mix was monitored to capture the exothermic reaction that takes place during the hardening process. The FLIR SC640 thermal camera was used simultaneously during the UPV tests to record the temperature change. Consequently, these measurements were also obtained three minutes after initial contact with water. Fig. 13 shows the evolution of samples temperatures, where the error clouds represent the standard deviation. The time needed to reach the maximum temperature during the hydration process for each mix was recorded (Table 5), ranging between 63 % and 75 % of the

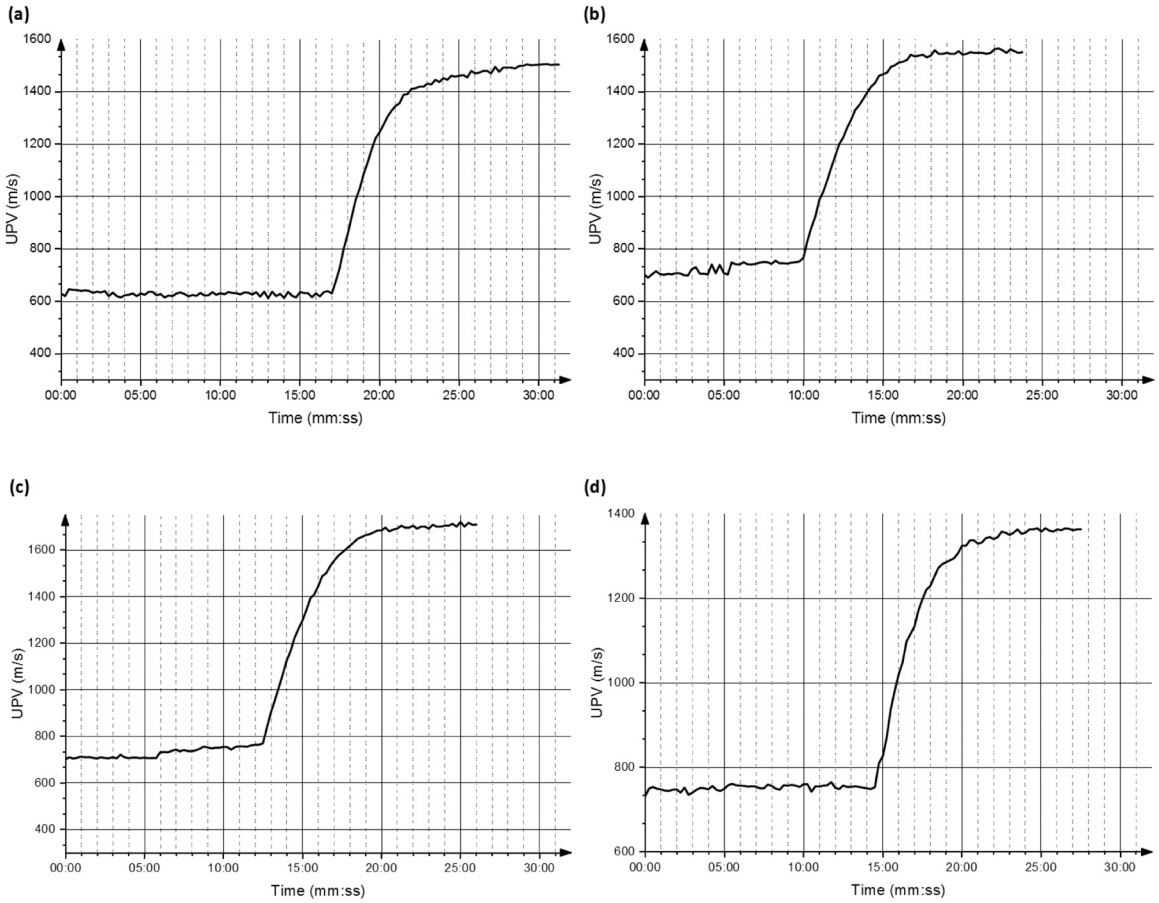

Fig. 12. The evolution of UPV as a function of time for mixes (a) 0 % NM, (b) 1 % NS, (c) 2 % NS, and (d) 3 % NS.

Table 4
Times for the UPV and Vicat needle tests for the four mixes.

Mixes	UPV Time (Minutes)	Vicat Needle Time (Minutes)
0 % NM	20.0 ± 0.8	19.4 ± 0.9
1 % NS	13.0 ± 0.4	13.2 ± 0.5
2 % NS	15.5 ± 0.6	15.0 ± 0.7
3 % NS	17.5 ± 0.3	18.0 ± 0.4

setting time indicating that energy released during the exothermic reaction takes place within the aforementioned window. This observed behavior corroborates results from the UPV and Vicat needle tests, which indicate that nano-silica tends to increase the hydration rate of the geopolymer mix. Moreover, as the setting time decreases (i.e., the rate of polymerization increases), the maximum temperature reached is higher because the exothermic energy release is concentrated within a shorter period. Temperature evolution due to the exothermic hydration reaction had been used to monitor the geopolymerization process, breaking down the kinetics of geopolymer synthesis into three distinct stages: dissolution, polymerization, and transformation [75]. Fast setting Na-activated geopolymers display two well-defined peaks of dissolution and polymerization, which occur approximately between 3 and 5 min and 15–20 min, respectively [76]. For the mixtures evaluated in this study, these two peaks appear to converge and coincide with a similar timeframe for the heat discharge process, concluding after about 15–20 min. Although these thermal patterns align, there is a noticeable scarcity of data regarding the temperature profile evolution for Na/K-activated geopolymers. This data could be crucial in identifying excessive heat and potential dehydration and cracking within the geopolymer matrix.

3.2.2. Flowability measurements

The optimized geopolymer mix of 1 % NS determined from the above tests was assessed for printability using flowability tests. Initially, the shear stress evolution of 1 % NS with time was found at a constant speed of 1200 rpm (Fig. 14). The printing tests were conducted for the same mix in order to determine the upper and lower bounds of the shear-strength-based printability range according

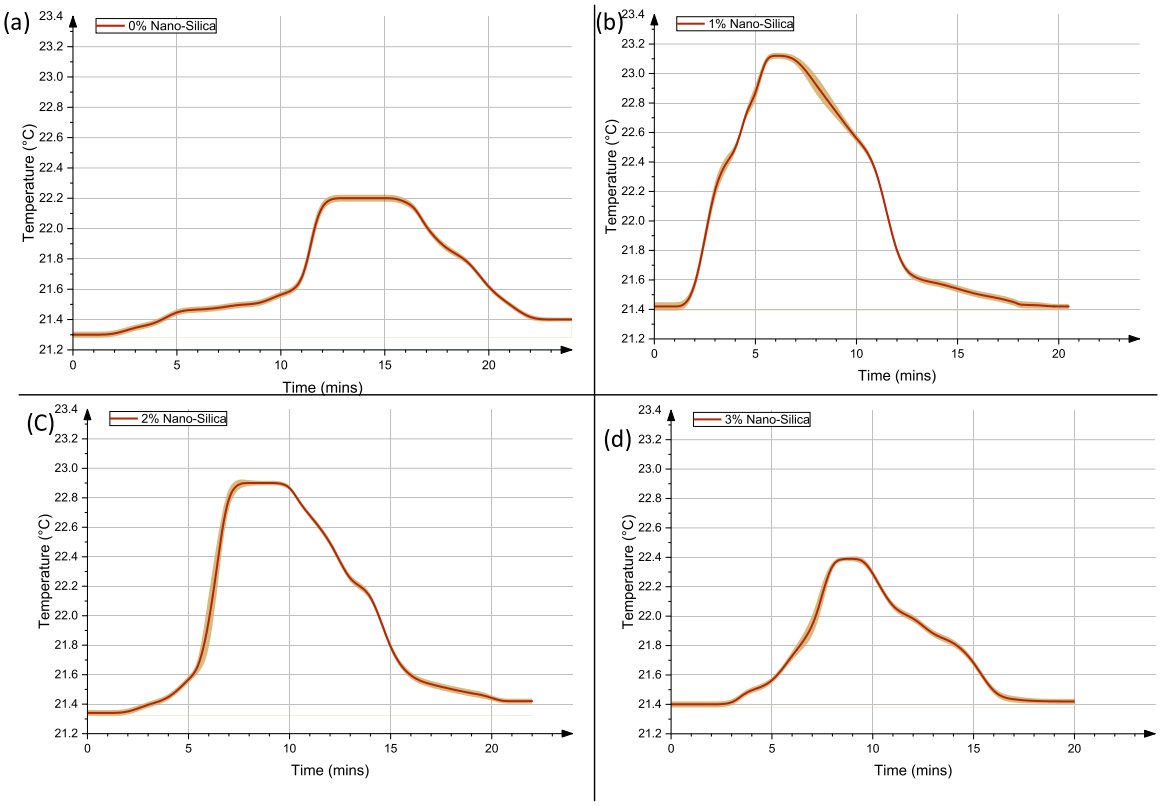

Fig. 13. Evolution of temperature as a function of time for mixes with (a) 0 % NM, (b) 1 % NS, (c) 2 % NS, and (d) 3 % NS.

Table 5
Summary of the thermal energy analysis for mixtures with nano-silica additives.

Mixes	Maximum Temperature during Hydration (°C)	Time to Maximum Temperature (Minutes)	Percentage of Setting Time
0 % NM	22.20 ± 0.03	15.0 ± 0.8	75.0 %
1 % NS	23.12 ± 0.07	8.5 ± 0.3	65.4 %
2 % NS	22.90 ± 0.09	10.0 ± 0.5	64.5 %
3 % NS	22.39 ± 0.05	11.0 ± 0.5	62.9 %

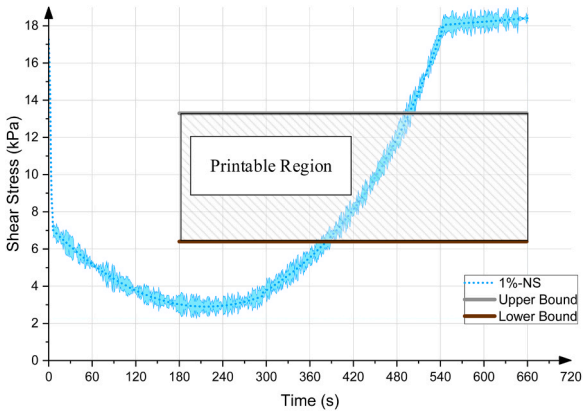

Fig. 14. Shear evolution as a function of time for 1 % NS at a constant speed of 1200 rpm.

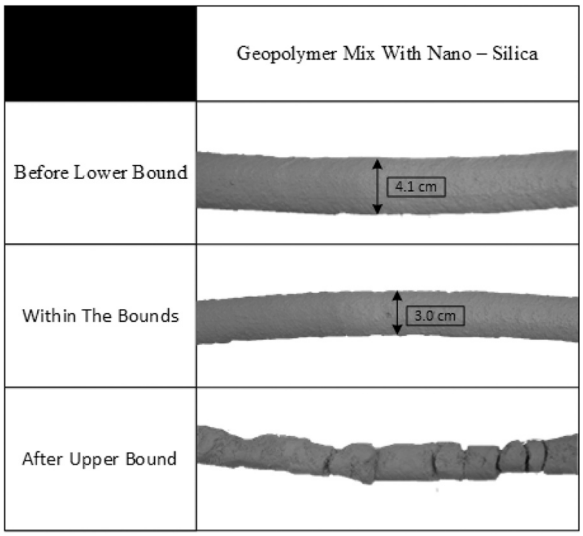

Fig. 15. Examples of filaments below, within, and above the upper bound of printing with the corresponding layer thickness.

Table 6
Average early age compressive strength values.

Time (Minutes)	Compressive Strength (MPa)
9	0.23 ± 0.05
11.5	0.38 ± 0.03
15	0.41 ± 0.01
20	0.44 ± 0.02
30	0.50 ± 0.03
40	0.54 ± 0.03
45	0.57 ± 0.04
50	0.61 ± 0.02
60	0.64 ± 0.01

to the test presented in Mortada et al. [64]. Whilst the lower bound is a function of the desired layer thickness, the upper bound is defined as the shear stress that would induce cracks or gaps within the printed layers. Initial conditions of the rheological test were replicated, with three minutes of mixing undertaken before initiating pumping of the geopolymer mix. Single-layer filaments were then deposited, with the thickness of filaments measured continuously. The onset of the acceptable layer thickness for the lower bound of printability was 3.5 cm, with the onset of the upper bound corresponding with the occurrence of breakages and gaps in the printed filament. The time corresponding to each of the bounds was correlated with its corresponding shear strength value (Fig. 14). Fig. 15 presents examples of the filaments below the lower bound, within the printability range, and above the upper bound, with their corresponding layer thicknesses. The pattern seen in Fig. 14 is consistent with the anticipated evolution of shear stress in a setting material. The initial drop in shear stress (up to 240 s) can be attributed to the mixing process that occurs before dissolution begins, as indicated by the initial temperature rise shown in Fig. 13. The following increase in shear stress results from the dissolution and polymerization process of the geopolymer, which leads to material hardening. This process persists until the material solidifies, leading to a steady shear rate that mirrors the torque needed to mix the solid geopolymer aggregates. Geopolymers and solidifying polymers typically exhibit a similar pattern of stress evolution [77].

3.2.3. Buildability test

The optimized mixture (1 % NS) was assessed for its buildability by measuring its early-age compressive strength. Early age is characterized by the time period immediately after layer deposition in order to assess the evolving mechanical properties during printing. In this study, the initial time of testing was 9 min after mixing, which corresponded to the onset of the lower bound of the printable region found in the flowability tests (see Fig. 14). A second test was conducted at 11.5 min after mixing, corresponding to the onset of the upper bound of the printability range (see Fig. 14). Subsequent tests were performed at 5-minute and 10-minute intervals, to map the evolution of the material's compressive strength post-deposition. Nine 50-mm cubic specimens were prepared and tested based on the ASTM C109/109 M standard. Three different trials were conducted, with compressive strength for each time interval determined as the mean of each of the three corresponding tests (Table 6).

Further analysis was conducted to assess the plastic stability of the material during printing. The stress exerted per meter of a printed layer was calculated, according to $\sigma = \frac{m \times 9.8 \frac{m}{s^2}}{A}$ and by taking into consideration the parameters shown in Table 6. The stress

Table 7
Parameters for assessing the stress applied by a 1-m printed layer.

Parameter	Measurement
Density	2000 kg/m^3
Layer height	2 cm
Maximum layer thickness	3.5 cm
Layer length	100 cm
Layer volume	0.0007 m^3
Mass per layer (m)	1.4 kg
Area of contact (A)	0.035 m^2
Stress per deposited layer	0.00039 MPa

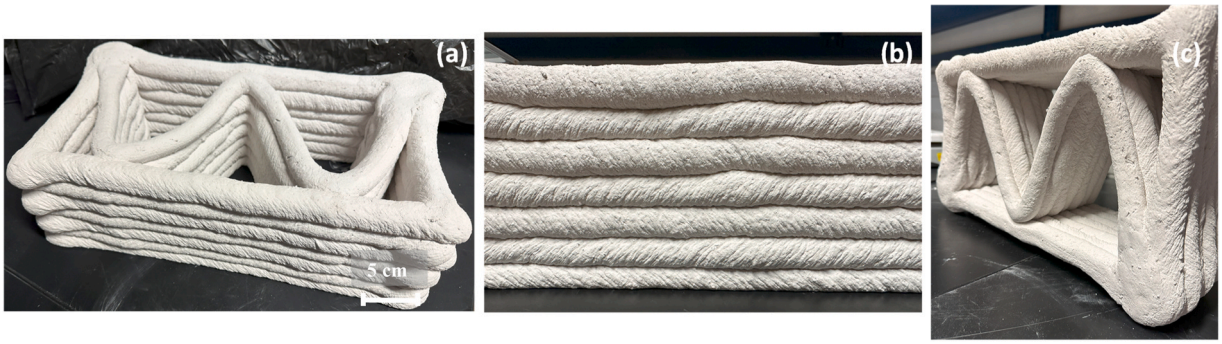

Fig. 16. The printed model of the geopolymer mixture.

applied by a deposited layer of a 1-m length was 0.00039 MPa, suggesting that 589 layers can be applied before the minimum compressive strength of 0.23 MPa is reached. Therefore, given that the strength of the geopolymer concrete continuously increases and that the minimum compressive strength was taken into consideration in this analysis, it can be surmised that plastic failure over the print life cycle with the selected geopolymer mixture is unlikely with the tested print parameters (Table 7).

Finally, the printability assessment of the geopolymer mix was completed by printing an 80-cm by 40-cm rectangular wall section (Fig. 16). This was successfully completed as the material was extruded continuously without any defects. Moreover, the deposited layers were able to withstand the load exerted on them without any collapse and buckling taking place, highlighting the suitability of the material to achieve successful prints. However, only seven layers of the model were printed due to the limitation of the quantity of material that could be stored in the batch mixer used. Further improvements to the print can be made by optimizing the print process parameters, such as eliminating the slight pause that is exhibited at the corners which led to excess material deposition.

4. Conclusions

In this study, a geopolymer mixture containing construction waste materials, slag, and a $Ca(OH)_2$ alkaline activator was developed and investigated as a sustainable material for additive manufacturing (AM). Additionally, the impact of nano-materials on geopolymer material properties, and the printability of an optimized nano-material modulated geopolymer mixture evaluated. The following conclusions are derived from this study:

- The geopolymer mixture had a 28-day compressive strength of 42 MPa, thus making it comparable to commonly used Na/K-based geopolymers mixtures.
- The addition of 1 wt % nano-clay (NC) had the largest effect in reducing thermal conductivity of the geopolymer mixture by 28 %, which was reduced from 0.709 W/mK to 0.505 W/mK. The addition of larger doses of NC resulted in an increased interconnectivity of the microstructure (i.e. fewer pores are present to disturb the thermal energy flow throughout the sample), and caused an increase of thermal conductivity.
- The addition of 1 wt % nano-silica (NS) had the largest effect in reducing of the setting time of the geopolymer mixture (35 %), reducing setting times from 20 to 13 min. The addition of larger doses of NS resulted in oversaturation of the matrix which reduced the efficacy of the additives and increased the setting time of the samples.
- An optimized mixture, 1 wt % NS and 1 wt % NC, encompassing the largest reductions in setting time and thermal conductivity was assessed for use in additive manufacturing (AM). Printability assessments were conducted using the flowability and buildability parameters, with optimized parameters used to successfully fabricate a test model using concrete 3D printing.

Notably, the use of $Ca(OH)_2$ as a sole alkaline activator is novel within the geopolymer literature, addressing many of the major disadvantages of existing geopolymer mixtures. The use of nano-materials resulted in enhanced printing and thermal properties (i.e. reduced setting time and thermal conductivity) to achieve an energy-efficient material suitable for utilization in AM applications.

Future work will focus on enhancing the mechanical properties, such as compressive strength, durability, and shrinkage, of the geopolymer mixture. The addition of fiber reinforcement to this mixture could help achieve this enhancement in mechanical properties and could extend the utility of the mixture to structural load-bearing members.

Declaration of Competing Interest

The authors declare that they have no known competing financial interests or personal relationships that could have appeared to influence the work reported in this paper.

Data Availability

Data will be made available on request.

Acknowledgements

This publication was made possible by funding (AICC02–0429-190014: Additive Manufacturing of Concrete for Sustainable Construction using Locally Developed Materials) from the Qatar National Research Fund (QNRF – a member of The Qatar Foundation). The statements made herein are solely the responsibility of the authors. The authors are thankful to the Arab Center for Engineering Studies (ACES), Doha, Qatar for carrying out some of the mechanical testing. Open Access funding provided by Qatar National Library.

References

[1] W. Gyadu-Asiedu, A. Ampadu-Asiamah, A. Fokuo-Kusi, A framework for systemic sustainable construction industry development (SSCID), Discov. Sustain. 2 (1) (2021) 25.
[2] Jennifer Layke et al. Accelerating building efficiency: Eight actions for urban leaders. In: World Resources Institute, wri.org/buildingefficiency (2016).
[3] M. Aslam, B. Huang, L. Cui, Review of construction and demolition waste management in China and USA, J. Environ. Manag. 264 (2020), 110445.
[4] M. Alsheyab, Recycling of construction and demolition waste and its impact on climate change and sustainable development, Int. J. Environ. Sci. Technol. 19 (3) (2022) 2129–2138.
[5] D. Ioannidou, G. Meylan, G. Sonnemann, G. Habert, Is gravel becoming scarce? Evaluating the local criticality of construction aggregates, Resour. Conserv. Recycl. 126 (2017) 25–33.
[6] P. Peduzzi, Sand, rarer than one thinks, Environ. Dev. 11 (2014) 208–218.
[7] J. Di Filippo, J. Karpman, J.R. DeShazo, The impacts of policies to reduce CO_2 emissions within the concrete supply chain, Cem. Concr. Compos. 101 (2019) 67–82.
[8] A.A.A. Samad, J. Hadipramana, N. Mohamad, A.Z.M. Ali, N. Ali, W.I. Goh, K.F. Tee, Development of green concrete from agricultural and construction waste. Transition towards 100% Renewable Energy, Springer, Cham, Switzerland, 2018, pp. 399–410.
[9] K. Kupwade-Patil, E.N. Allouche, Impact of alkali silica reaction on fly ash-based geopolymer concrete, J. Mater. Civ. Eng. 25 (2012) 131–139.
[10] Meyer, The greening of the concrete industry, C. Meyer Cem. Concr. Compos. 31 (2009) 601–605.
[11] T. Xie, P. Visintin, X.-Y. Zhao, R.J. Gravina, Mix design and mechanical properties of geopolymer and alkali activated concretes: review of the state-of-the-art and the development of a new unified approach, Constr. Build. Mater. 256 (2020), https://doi.org/10.1016/j.conbuildmat.2020.119380.
[12] K. Ramujee, P. Malasani, Mechanical properties of geopolymer concrete composites, Mater. Today.: Proc. 4 (2017) 2937–2945, https://doi.org/10.1016/j.matpr.2017.02.175.
[13] A.A. Mohammed, H.U. Ahmed, A. Mosavi, Survey of mechanical properties of geopolymer concrete: a comprehensive review and data analysis, Aug 20, Materials (Basel) 14 (16) (2021) 4690, https://doi.org/10.3390/ma14164690. PMID: 34443212; PMCID: PMC8398852..
[14] M.A. Zhang, A multiscale investigation of reaction kinetics, phase formation, and mechanical properties of metakaolin geopolymer, Cem. Concr. Comp. 78 (2017) 21–32, https://doi.org/10.1016/j.cemconcomp.2016.12.010.
[15] G.B. Singh, V.L. Kolluru, Subramaniam evaluation of sodium content and sodium hydroxide molarity on compressive strength of alkali activated low-calcium fly ash, Cem. Concr. Comp. 81 (2017) 122–132, https://doi.org/10.1016/j.cemconcomp.2017.05.001.
[16] A. Rehman, V. Sglavo, 3D printing of geopolymer-based concrete for building applications, Rapid Prototyp. J. (2020), https://doi.org/10.1108/RPJ-09-2019-0244.
[17] E. El-Seidy, M. Chougan, M. Sambucci, M.J. Al-Kheetan, M. Valente, S.H. Ghaffar, Lightweight alkali-activated materials and ordinary Portland cement composites using recycled polyvinyl chloride and waste glass aggregates to fully replace natural sand, Constr. Build. Mater. 368 (2023), 130399.
[18] E. El-Seidy, M. Sambucci, M. Chougan, M.J. Al-Kheetan, M. Valente, S.H. Ghaffar, Mechanical and physical characteristics of alkali- activated mortars incorporated with recycled polyvinyl chloride and rubber aggregates, issn: 2352-7102, J. Build. Eng. 60 (2022), 105043, https://doi.org/10.1016/j.jobe.2022.105043.
[19] K. Cuevas, M. Chougan, F. Martin, S.H. Ghaffar, D. Stephan, P. Sikora, 3D printable lightweight cementitious composites with incorporated waste glass aggregates and expanded microspheres – rheological, thermal and mechanical properties, issn: 2352-7102, J. Build. Eng. 44 (2021), 102718, https://doi.org/10.1016/j.jobe.2021.102718.
[20] M. Valente, M. Sambucci, M. Chougan, S.H. Ghaffar, Composite alkali-activated materials with waste tire rubber designed for additive manufacturing: an eco-sustainable and energy saving approach, J. Mater. Res. Technol. 24 (2023) 3098–3117.
[21] M. Chougan, S.H. Ghaffar, P. Sikora, S.Y. Chung, T. Rucinska, D. Stephan, A. Albar, M.R. Swash, Investigation of additive incorporation on rheological, microstructural and mechanical properties of 3D printable alkali-activated materials, Mater. Des. 202 (2021), 109574.
[22] M. Chougan, S.H. Ghaffar, B. Nematollahi, P. Sikora, T. Dorn, D. Stephan, A. Albar, M.J. Al-Kheetan, Effect of natural and calcined halloysite clay minerals as low-cost additives on the performance of 3D-printed alkali-activated materials, Mater. Des. 223 (2022), 111183.
[23] D. Asprone, F. Auricchio, C. Menna, V. Mercuri, 3D printing of reinforced concrete elements: technology and design approach, Constr. Build. Mater. 165 (2018) 218–231.
[24] E. Lloret, A.R. Shahab, M. Linus, R.J. Flatt, Complex concrete structures: merging existing casting techniques with digital fabrication, Comput. -Aided Des. 60 (2015) 40–49.
[25] A. Karaki, M. Mohammad, E. Masad, M. Khraisheh, Theoretical and computational modeling of thermal properties of lightweight concrete, Case Stud. Therm. Eng. 28 (2021), 101683.
[26] I. Sartori, A.G. Hestnes, Energy use in the life cycle of conventional and low-energy buildings: a review article, Energy Build. 39 (3) (2007) 249–257.
[27] A. Passer, C. Ouellet-Plamondon, P. Kenneally, V. John, G. Habert, The impact of future scenarios on building refurbishment strategies towards plus energy buildings, Energy Build. 124 (2016) 153–163.

[28] M. Rock, M.R.M. Saade, M. Balouktsi, F.N. Rasmussen, Embodied GHG emissions of buildings—the hidden challenge for effective climate change mitigation, Appl. Energy 258 (2020), 114107.
[29] B. Tekle, L. Hertwig, K. Holschemacher, Setting time and strength monitoring of alkali-activated cement mixtures by ultrasonic testing, Materials 14 (2021) 1889.
[30] C. Shi, A.F. Jiménez, A. Palomo, New cements for the 21st century: the pursuit of an alternative to Portland cement, Cem. Concr. Res. 41 (7) (2011) 750–763, https://doi.org/10.1016/j.cemconres.2011.03.016.
[31] J. Matsimbe, M. Dinka, D. Olukanni, I. Musonda, Geopolymer: a systematic review of methodologies, Materials 15 (2022) 6852, https://doi.org/10.3390/ma15196852.
[32] H. Castillo, H. Collado, T. Droguett, S. Sánchez, M. Vesely, P. Garrido, S. Palma, Factors affecting the compressive strength of geopolymers: a review, Minerals 11 (12) (2021) 1317.
[33] M. Nodehi, V. Taghvaee, Alkali-activated materials and geopolymer: a review of common precursors and activators addressing circular economy, Circ. Econ. Sustain. 2 (1) (2021) 165–196.
[34] S. Zhou, C. Tan, Y. Gao, Y. Li, S. Guo, One-part alkali activated slag using Ca(OH)2 and Na2CO3 instead of NaOH as activator: More excellent compressive strength and microstructure, Mater. Res. Express 8 (8) (2021), 085501.
[35] K. Alventosa, C. White, The effects of calcium hydroxide and activator chemistry on alkali-activated metakaolin pastes, Cem. Concr. Res. 145 (2021), 106453.
[36] C. Yip, G. Lukey, J. Van Deventer, The coexistence of geopolymeric gel and calcium silicate hydrate at the early stage of alkaline activation, Cem. Concr. Res. 35 (2005) 1688–1697, https://doi.org/10.1016/j.cemconres.2004.10.042.
[37] A. Marsh, T. Yang, S. Adu-Amankwah, S. Bernal, Utilization of metallurgical wastes as raw materials for manufacturing alkali-activated cements, Waste Byprod. Cem. - Based Mater. (2021) 335–383.
[38] Seyed Ali Nabavi Maria Erans, Vasilije Manovic, Carbonation of lime-based materials under ambient conditions for direct air capture, J. Clean. Prod. 242 (2020), 118330.
[39] Dawid P. Hanak, Vasilije Manovic, Combined heat and power generation with lime production for direct air capture, Energy Convers. Manag. 160 (2018) 455–466.
[40] H. Assaedi, F.U.A. Shaikh, I.M. Low, Characterizations of flax fabric reinforced nanoclay-geopolymer composites, Compos. B Eng. 95 (2016) 412–422, https://doi.org/10.1016/j.compositesb.2016.04.007.
[41] H. Assaedi, F.U.A. Shaikh, I.M. Low, Effect of nano-clay on mechanical and thermal properties of geopolymer, J. Asian Ceram. Soc. 4 (1) (2016) 19–28, https://doi.org/10.1016/j.jascer.2015.10.004.
[42] N.B. Singh, S.K. Saxena, M. Kumar, Effect of nano-materials on the properties of geopolymer mortars and concrete, Mater. Today.: Proc. 5 (3) (2018) 9035–9040.
[43] D. Adak, M. Sarkar, S. Mandal, Effect of nano-silica on strength and durability of fly ash based geopolymer mortar, Constr. Build. Mater. 70 (2014) 453–459.
[44] H.U. Ahmed, A.S. Mohammed, R.H. Faraj, S.M.A. Qaidi, A.A. Mohammed, Compressive strength of geopolymer concrete modified with nano-silica: experimental and modeling investigations, Case Stud. Constr. Mater. 16 (2022).
[45] M. Aly, M.S.J. Hashmi, A.G. Olabi, M. Messeiry, A.I. Hussain, Effect of nano clay particles on mechanical, thermal and physical behaviours of waste-glass cement mortars, Mater. Sci. Eng.: A 528 (27) (2011) 7991–7998.
[46] M.A.M. Langaroudi, Y. Mohammadi, Effect of nano-clay on workability, mechanical, and durability properties of self-consolidating concrete containing mineral admixtures, Constr. Build. Mater. 191 (2018) 619–634.
[47] H. Assaedi, F.U.A. Shaikh, I.M. Low, Effect of nano-clay on mechanical and thermal properties of geopolymer, J. Asian Ceram. Soc. 4 (1) (2016) 19–28.
[48] S. Naskar, A.K. Chakraborty, Effect of nano materials in geopolymer concrete, Perspect. Sci. 8 (2016) 273–275.
[49] H. Assaedi, F.U.A. Shaikh, I.M. Low, Influence of mixing methods of nano silica on the microstructural and mechanical properties of flax fabric reinforced geopolymer composites, Constr. Build. Mater. 123 (2016) 541–552, https://doi.org/10.1016/j.conbuildmat.2016.07.049.
[50] R. Polat, R. Demirboğa, W.H. Khushefati, Effects of nano and micro size of Cao and mgo, nano-clay and expanded perlite aggregate on the autogenous shrinkage of mortar, Constr. Build. Mater. 81 (2015) 268–275.
[51] H. Assaedi, F.U.A. Shaikh, I.M. Low, Effect of nano-clay on mechanical and thermal properties of geopolymer, J. Asian Ceram. Soc. 4 (1) (2016) 19–28, https://doi.org/10.1016/j.jascer.2015.10.004.
[52] S. Kawashima, K. Wang, R.D. Ferron, J.H. Kim, A review of the effect of nanoclays on the fresh and hardened properties of cement-based materials, Cem. Concr. Res. 147 (2021), 106502, https://doi.org/10.1016/j.cemconres.2021.106502.
[53] H. Khater, Effect of nano-clay on alkali activated water-cooled slag geopolymer, Br. J. Appl. Sci. Technol. 3 (4) (2013) 764–776, https://doi.org/10.9734/bjast/2013/2690.
[54] M.R. Irshidat, M.H. Al-Saleh, Influence of nanoclay on the properties and morphology of cement mortar, KSCE J. Civ. Eng. 22 (10) (2018) 4056–4063, https://doi.org/10.1007/s12205-018-1642-x.
[55] P. Aggarwal, R.P. Singh, Y. Aggarwal, Use of nano-silica in cement based materials—a review, Cogent Eng. 2 (2015) 1078018, https://doi.org/10.1080/23311916.2015.1078018.
[56] K. Gao, K.-L. Lin, D. Wang, C.-L. Hwang, H.-S. Shiu, Y.-M. Chang, T.-W. Cheng, Effects SiO_2/Na_2O molar ratio on mechanical properties and the microstructure of nano-SiO_2 metakaolin-based geopolymers, Constr. Build. Mater. 53 (2014) 503–510, https://doi.org/10.1016/j.conbuildmat.2013.12.003.
[57] G. Roviello, L. Ricciotti, O. Tarallo, C. Ferone, F. Colangelo, V. Roviello, R. Cioffi, Innovative fly ash geopolymer-epoxy composites: Preparation, microstructure and mechanical properties, Materials 9 (2016) 461, https://doi.org/10.3390/ma9060461.
[58] M. Chougan, S.H. Ghaffar, M. Jahanzat, A. Albar, N. Mujaddedi, R. Swash, The influence of nano-additives in strengthening mechanical performance of 3D printed multi-binder geopolymer composites. https://doi.org/10.1016/j.conbuildmat.2020.118928.
[59] J.C. Kuri, S. Majhi, P.K. Sarker, A. Mukherjee, Microstructural and non-destructive investigation of the effect of high temperature exposure on ground ferronickel slag blended fly ash geopolymer mortars, J. Build. Eng. 43 (2021), 103099.
[60] ASTM C109/C109M, Standard Test Method for Compressive Strength of Hydraulic Cement Mortars (Using 2-in. or [50 mm] Cube Specimens), ASTM International, West Conshohocken, PA, 2021.
[61] K. Kumar, M. Shashi, V. Keesara, Therm. Remote Sens. Early Age Concr. Strength Estim. (2019), https://doi.org/10.1007/978-981-13-7067-0_4.
[62] ASTM D5334-22a, Standard Test Method for Determination of Thermal Conductivity of Soil and Rock by Thermal Needle Probe Procedure, ASTM International, 2022.
[63] ASTM C642–21: Standard Test Method for Density, Absorption, and Voids in Hardened Concrete, ASTM International, Book of Standards Volume 04.02, Developed by Subcommittee C09.66, p. 3. doi: 10.1520/C0642–21 ICS Code: 91.100.30.
[64] Y. Mortada, M. Mohammad, B. Mansoor, Z. Grasley, E. Masad, Development of test methods to evaluate the printability of concrete materials for additive manufacturing, Materials 15 (2022) 6486, https://doi.org/10.3390/ma15186486.
[65] ASTM C191-21, Standard Test Methods for Time of Setting of Hydraulic Cement by Vicat Needle, ASTM International, West Conshohocken, PA, 2021.
[66] R. Mohamed, R.Abd Razak, Investigation of heat released during geopolymerization with fly ash based geopolymer, IOP Conf. Ser.: Mater. Sci. Eng. 551 (2019) 012093. doi: 10.1088/1757–899X/551/1/012093.
[67] S.K. Rahman, R. Al-Ameri, A newly developed self-compacting geopolymer concrete under ambient condition, issn: 0950-0618, Constr. Build. Mater. 267 (2021), 121822, https://doi.org/10.1016/j.conbuildmat.2020.121822.
[68] L.S. Wong, Durability performance of geopolymer concrete: a review, Polymers 14.5 (2022) 868.39.
[69] N.A.M. Mortar, H. Kamarudin, R.A. Rafiza, T.A.F. Meor, M. Rosnita, Compressive strength of fly ash geopolymer concrete by varying sodium hydroxide molarity and aggregate to binder ratio, IOP Conference Series: Materials Science and Engineering 864.1 (May 2020) 012037. doi: 10.1088/1757–899X/864/1/012037.
[70] M. Valente, M. Sambucci, M. Chougan, S.H. Ghaffar, Composite alkali-activated materials with waste tire rubber designed for additive manufacturing: an eco-sustainable and energy saving approach, J. Mater. Res. Technol. 24 (2023) 3098–3117.

[71] Rui He, Nan Dai, Zhenjun Wang, Thermal and mechanical properties of geopolymers exposed to high temperature: a literature review, Adv. Civ. Eng. 2020 (2020) 1–17.
[72] Fatimah Azzahran Abdullah', S., Yun-Ming, L., Mustafa Al Bakri Abdullah, M., Cheng-Yong, H. and Zulkifly, K. Mechanical properties and thermal conductivity of lightweight foamed geopolymer concretes. In: IOP Conference Series: Materials Science and Engineering. Vol. 551. 1. IOP Publishing. 2019, p. 012089.
[73] A. Buades, B. Coll, J.M. Morel, Non-local means denoising, Image Process. Line 1 (2011) 208–212.
[74] Xinhui Liu, Chunfeng Hu, Longsheng Chu, Microstructure, compressive strength and sound insulation property of fly ash-based geopolymeric foams with silica fume as foaming agent. Materials 13 (14) (2020) 3215.
[75] Rosnita Mohamed, Rafiza Abd Razak, Mohd Mustafa Al. Bakri Abdullah, A review on heat released in early geopolymerization by calorimetric study, in: Materials Science Forum, vol. 967, Trans Tech Publications Ltd, 2019.
[76] Mohamed, Rosnita, Rafiza Abd Razak, Mohd Mustafa Al. Bakri Abdullah, Raa Khimi Shuib, Nurul Aida Mohd Mortar, Warid Wazien Ahmad Zailani. Investigation of heat released during geopolymerization with fly ash based geopolymer. IOP Conference Series: Materials Science and Engineering. vol. 551. No. 1. IOP Publishing, 2019.
[77] Qiang Yuan, Dajun Zhou, Kamal H. Khayat, Dimitri Feys, Caijun Shi, On the measurement of evolution of structural build-up of cement paste with time by static yield stress test vs. small amplitude oscillatory shear test, Cem. Concr. Res. 99 (2017) 183–189.